

Stabilization of Ruthenium Sensitizers to TiO₂ Surfaces through Cooperative Anchoring Groups

Douglas G. Brown, Phil A. Schauer, Javier Borau-Garcia, Brandon R. Fancy, and Curtis P. Berlinguette*

Department of Chemistry, University of Calgary, 2500 University Drive NW, Calgary, Alberta, Canada T2N 1N4

S Supporting Information

ABSTRACT: Cooperative binding of a bis(tridentate) ruthenium(II) complex to a TiO₂ surface through carboxylate and phosphonate groups is demonstrated to be an effective method for achieving a robust anchoring motif in aqueous media while maintaining charge transfer from the dye into the semiconductor. The realization of these complementary goals has broad implications for solar cells and (photo)electrocatalytic schemes.

The dye-sensitized solar cell (DSSC) is a promising advanced photovoltaic (PV) technology. The long-term stability of DSSCs nonetheless remains a significant impediment to commercialization because of issues with hermetic sealing of the liquid electrolyte and the consequent degradation and desorption of the dye.^{1–4} While recent advances in solid-state hole-transport materials (e.g., perovskites, polymers) have provided a viable pathway for bypassing liquid-phase electrolytes,^{5,6} charge-transport limitations have to date confined efficiencies to less than those of liquid electrolytes. The long-term stability of the sensitizer represents another critical problem:^{3,7} the current set of commercially relevant dyes that are related to [Ru(dcbpy)₂(NCS)₂] (dcbpy = 4,4'-dicarboxy-2,2'-bipyridine; N3) are susceptible to degradation through dissociation of the labile NCS[−] ligands. In recognition of these shortcomings, our research program and others have sought to replace these monodentate ligands with *chelating* bidentate and tridentate ligands without compromising the device performance.^{8,9} A second key stability issue for conventional DSSCs is dye desorption from the TiO₂ surface caused by hydrolysis of the acid groups that bind the dye to the semiconductor and/or competitive binding with adventitious hydroxide. The electrolyte matrix in state-of-the-art devices thus requires rigorous exclusion of water for efficient operation over prolonged periods of time. It would therefore be beneficial to use dyes with anchoring groups that are not compromised by water while maintaining efficient injection.

All of the high-performance DSSC dyes in the literature contain at least one carboxylate anchoring group because these groups provide intimate electronic coupling between the dye and the TiO₂ semiconductor.¹ The aforementioned susceptibility of the carboxylate–TiO₂ linkage to hydrolysis is typically addressed by spatially blocking water from reaching the titania/carboxylate interface using aliphatic units.^{10,11} Unfortunately, replacing the carboxylic acid group with alternate, more robust chemical functionalities [e.g., –B(OH)₂, –NO₂, –OH, –P(O)(OH)₂, –S(O)₂(OH), etc.] often introduces problems

relating to dye aggregation and/or interfacial electronic phenomena.¹² The phosphonate functionality, for example, has received attention as an alternative to the carboxylate moiety because of the 5–10-fold increase in binding affinity for TiO₂, but the charge-injection rates are compromised by the tetrahedral phosphorous center.^{13–20}

We therefore set out to take advantage of the efficient electron injection mediated by a carboxylate linker while simultaneously exploiting the phosphonate functionality for increased surface binding stability. The underlying basis of this simple strategy is that the carboxylate moiety needs only to be positioned on the ligand that is involved in charge transfer to the TiO₂, while the phosphonate moieties can be installed on the opposing ligand that does not need to participate directly in the injection process. We prepared four model complexes (Figure 1) containing a carboxylate anchoring group (1 and 2), phosphonate anchoring groups (3), or both (4) to demonstrate this strategy. It was found that the cooperative binding modes of 4 exhibit a significantly greater stability on TiO₂ relative to N3 while also producing a higher efficiency in the DSSC relative to 1–3. We contend that this strategy will find broad use in a myriad of sensitization and catalytic applications where molecules are attached to semiconducting surfaces.

Complexes 1–4 were synthesized in a manner analogous to a previously published route,²¹ and the final products were isolated in moderate yields. The UV–vis absorption spectrum of each of the corresponding ester derivatives (denoted as 1'–4', respectively) revealed a metal-to-ligand charge-transfer (MLCT) band centered at ca. 460 nm with an extinction coefficient on the order of 1.0 × 10⁴ M^{−1} cm^{−1} [Table 1 and Figure S7 in the Supporting Information (SI)]. The frontier molecular orbitals (MOs) determined by density functional theory (DFT) calculations²² indicate that the highest occupied MO (HOMO) is predominantly of metal character (ca. 60%), with the balance of the electron density residing more on the mesoionic carbene unit than on the terpyridine ligand (Tables S2 and S3 in the SI). The lowest unoccupied MOs (LUMOs) of 1' and 2' are clearly delocalized over the carboxyterpyridine ligand, whereas the LUMO of 3' is localized on the mesoionic carbene ligand because the terpyridine ligand without the carboxylate substituent is less strongly electron-withdrawing. The orbital picture is not as clear in the case of 4', wherein the LUMO and LUMO+1 are calculated to be within 0.01 eV of each other and have alternate delocalization over the mesoionic carbene and carboxyterpyridine ligands, respectively. Modeling

Received: November 12, 2012

Published: January 23, 2013

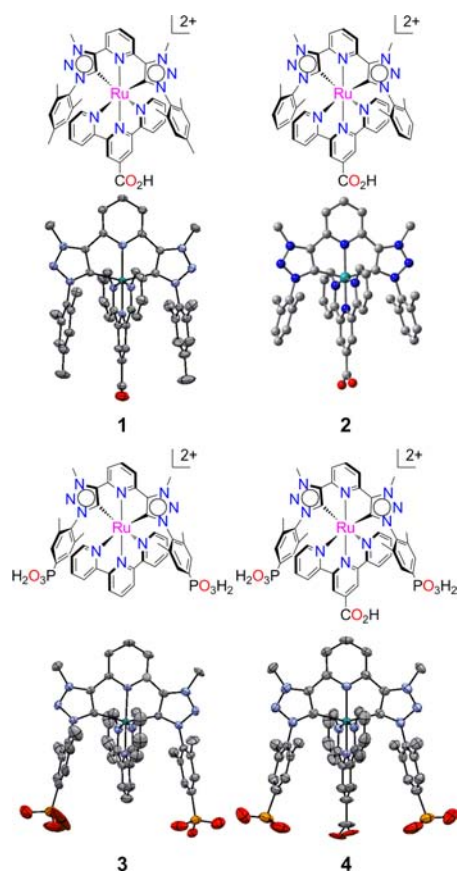


Figure 1. Ruthenium(II) complexes bearing a carboxylate anchoring group (1 and 2), phosphonate anchoring groups (3), or both (4). The counterion was BF_4^- in all cases. Depictions of the single-crystal X-ray structures of the ester derivatives 1', 3', and 4' and the DFT-optimized structure of 2' are shown to illustrate that the phosphonate and/or carboxylate functional groups are geometrically positioned for simultaneous surface binding. Colors: C, gray; N, blue; O, red; P, orange; Ru, teal. H atoms, anions, and methylcarboxylate and diethylphosphonate ester linkages have been omitted for clarity.

Table 1. Photophysical Data for Ester Precursors 1'–4'

	1'	2'	3'	4'
λ_{abs} (nm) ^{a,b}	472	469	458	461
ϵ ($10^4 \text{ M}^{-1} \text{ cm}^{-1}$)	1.0	1.0	1.0	1.0
λ_{em} (nm) ^c	688	649	647	694
τ (μs) ^c	1.72	7.38	6.02	2.12

^aMeasured in MeCN at 298 K. ^bAbsorption maximum of the lowest-energy MLCT band. ^cMeasured in deaerated MeCN at 298 K.

of the corresponding acid derivative 4 showed that the unoccupied frontier MOs exhibit a greater separation in energy (0.1 eV), with the LUMO localized on the carboxyterpyridine ligand. These calculations indicate that complexes 1, 2, and 4 are poised for electron injection through the anchoring carboxylate moiety.

The electrochemical and emission properties of 1'–4' were measured to ensure that the ground- and excited-state energy levels were appropriately suited for electron injection and dye regeneration in the DSSC. Cyclic voltammograms recorded on MeCN solutions of the complexes revealed single reversible metal-based oxidation waves at 1.2–1.3 V vs normal hydrogen electrode (NHE) (values indicated in Figure 2), with deviations commensurate with the number and positions of the acid

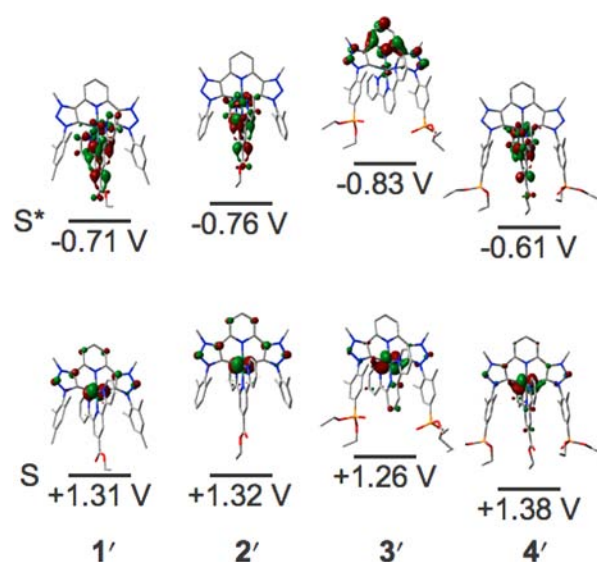


Figure 2. Energy level diagram for complexes 1'–4'. The ground-state energy (S) corresponds to the potential of the oxidative redox couple determined by cyclic voltammetry in 0.1 M $\text{NBu}_4\text{BF}_4/\text{MeCN}$ ($[\text{Fc}]^+ / [\text{Fc}]^0$ internal standard, +0.63 V vs NHE). The excited-state energy (S^*) corresponds to $S + E_{0-0}$, in which E_{0-0} is given by the intersection point of the absorption and emission curves, where the latter was normalized to the lowest-energy $^1\text{MLCT}$ band (see Figures S3–S6). The HOMOs and LUMOs (0.05 au) of the singlet states are plotted as representations of the ground and excited states, respectively. In the case of 4', the nearly isogenic LUMO+1 is shown because it is a better representation of the LUMO of 4.

groups. Square-wave voltammetry of the complexes bound to TiO_2 confirmed that the metal-based oxidative redox couples (Table S1) were positively shifted relative to the relevant one-electron couple of the iodide-based electrolyte (ca. 0.8 V vs NHE for $\text{I}^-/\text{I}_2^{\bullet-}$)²³ and thus appropriately positioned for dye regeneration. The potential of the emitting state was found to be more negative than -0.70 V vs NHE for 1–3 (Figure 2), which is adequate for effective electron injection into TiO_2 .¹ Complex 4 was determined to have an excited-state reduction potential of -0.61 V, which may not be sufficiently negative to mediate efficient charge transfer into TiO_2 . We postulate that the long excited-state lifetime of the complex may still accommodate efficient injection; experiments are underway to assess this possibility.

The PV performance parameters of devices containing each of the dyes bound to TiO_2 and iodide-based electrolytes were measured under simulated sunlight (Table 2). The absolute power conversion efficiencies (PCEs) were not remarkable, which was expected because of the poor spectral coverage of the dyes, but the trends in the data provide indirect information

Table 2. Photovoltaic Data for the Title Complexes and N3^a

	1	2	3	4	N3
V_{oc} (V)	0.33	0.14	0.16	0.41	0.61
J_{sc} (mA/cm^2)	0.09	1.2	0.12	0.97	10.7
fill factor	0.46	0.36	0.35	0.50	0.59
PCE (%)	0.01	0.07	0.007	0.2	3.9

^aCurrent density–voltage (J – V) curves were recorded on DSSCs under AM1.5 simulated sunlight with square titania anodes (active area = 0.88 cm^2 ; $12 \mu\text{m}$ active layer) and E50 electrolyte (see the SI for details).

about how charge collection is affected by the dye structure. Devices sensitized by **4**, for example, exhibited a modest PCE of 0.2%, but the output was still much greater than those of **1** and **2** and 2 orders of magnitude greater than that measured for **3**. The low PCE generated by **3** is likely due to the poorly positioned orbital character of the LUMO, which resides on the carbene fragment remote from the surface. The incident-photon-to-current efficiency (IPCE) data followed the same trend. These data clearly show that the phosphonate linkers attached to the carbene ligand do not facilitate meaningful light-induced charge transfer into the substrate despite energetics that are more conducive to the process. Spectrophotometric monitoring of dye uptake onto mesoporous TiO₂ substrates indicated similar dye loadings for **2** and **3** and enhanced dye loading for **4** (particularly rapid binding was observed for the dyes bearing the -PO₃²⁻ units), but the differences in the data may be due to the slightly lower surface coverages of **1**–**3** relative to that of **4** [which is also supported by the values of the open-circuit voltage (*V*_{OC})]. The dye loading of **1** was particularly poor, which we attribute to steric interactions between the *p*-methyl groups of the mesityl moieties and the TiO₂ surface that hinder the formation of strong bidentate carboxylate linkages (vide infra). Nevertheless, the dye with multiple anchoring groups exhibited the best PCE of the series, providing convincing evidence that charge injection is mediated by the carboxylate moiety even with the phosphonates present.

We set out to confirm the nature of the surface attachment of the dyes by interrogating the binding modes through diffuse-reflectance IR Fourier transform spectroscopy (DRIFTS) experiments. The spectra for the dyes attached to TiO₂ (denoted as **1**–**4**/TiO₂) are presented in Figure 3 (expanded views of these data are provided in Figure S8); the spectrum of **4** in KBr powder (denoted **4**/KBr) is also provided as a benchmark. The spectrum of **4**/TiO₂ clearly indicates the absence of the $\nu(\text{C}-\text{OH})$ and $\nu(\text{C}=\text{O})$ stretching modes at 1200 and 1720 cm⁻¹, respectively, that are present for **4**/KBr but does feature the characteristic carboxylate $\nu_s(\text{CO}_2)$ and

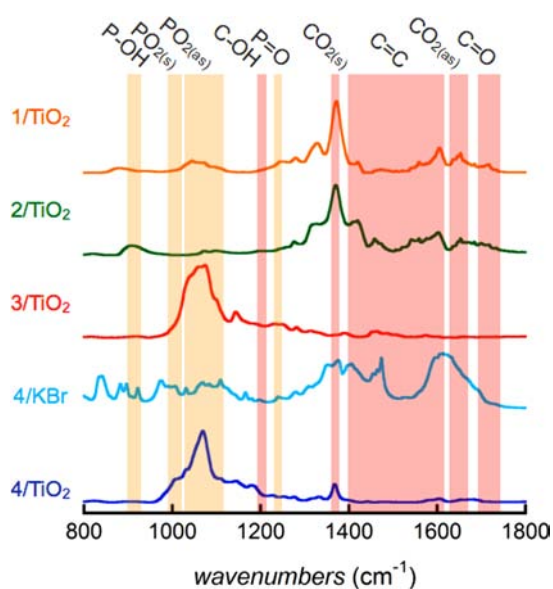


Figure 3. Kubelka–Munk DRIFTS spectra of **1**–**4**/TiO₂ and **4**/KBr. Subscripts “s” and “as” indicate symmetric and asymmetric, respectively.

$\nu_{\text{as}}(\text{CO}_2)$ modes at 1370 and ca. 1630 cm⁻¹, respectively. The ~ 260 cm⁻¹ difference between the symmetric and asymmetric carboxylate modes is consistent with a bidentate chelating/bridging attachment to the TiO₂ surface.^{14,24–27} Also evident from the spectrum of **4**/KBr are the $\nu(\text{P}-\text{OH})$ (935 cm⁻¹) and $\nu(\text{P}=\text{O})$ (1235 cm⁻¹) stretching modes, which are replaced in **4**/TiO₂ with $\nu(\text{PO}_3)$ modes clustered about 1050 cm⁻¹.^{14,28} The spectrum of **1**/TiO₂ reveals $\nu_s(\text{CO}_2)$ and $\nu_{\text{as}}(\text{CO}_2)$ stretching modes similar to those observed for **4**/TiO₂, although the signal at ca. 1700 cm⁻¹ is interpreted as a $\nu(\text{C}=\text{O})$ mode, indicating poor carboxylate binding for some proportion of the adsorbed dye molecules (which is corroborated by the poor dye loading and the results of the desorption studies). The carboxylate modes of **2**/TiO₂ are analogous to those of **4**/TiO₂, whereas the phosphonate modes of **3**/TiO₂ in the 950–1100 cm⁻¹ range deviate to a fair extent, offering little resolution of the differing phosphonate–titania binding interactions for **3** and **4** (vide infra). Nonetheless, because the carboxylate and phosphonate binding modes measured for **4**/TiO₂ were observed for **2**/TiO₂ and **3**/TiO₂, respectively, and deviate from those of **4**/KBr, we conclude that the different binding groups of **4** do indeed bind to TiO₂ in a cooperative fashion.

The dye loadings of the complexes on titania were inferred from relative differences in UV–vis absorption spectra (Figure S7). In solution, **1**–**4** have similar molar extinction coefficients (1.0×10^4 M⁻¹ cm⁻¹), and thus, differences in the absorption intensities for the stained substrates **1**–**4**/TiO₂ (on identical TiO₂/FTO anodes) may be correlated directly with the relative dye loadings. The dye loadings for the series followed the trend **1** < **2** < **3** < **4**. The presumably similar molecular footprints of the dyes suggest that the acid group does seem to influence the extent of dye loading. The low dye loading of **1** can be rationalized in terms of the steric impediment to dye attachment to the surface provided by the *p*-methyl substituents of the mesityl moieties. This conclusion is corroborated by the 2-fold higher dye loading of **2**, in which the *p*-methyl groups are replaced by H atoms. The higher loading for **3** relative to **2** is presumably due to the presence of two surface-binding moieties as opposed to the single carboxylate functionality of **1** and **2**, while the dye loading for the triply binding **4** is the highest among the series. While **4** (which features both phosphonate and carboxylate binding groups) exhibits a 2-fold or greater dye loading relative to those of **1**–**3**, these differences do not fully account for the relative differences in the PCEs.

The temporal stabilities of **1**–**4**/TiO₂ submerged in water (in the dark) were measured by spectrophotometric monitoring of the respective MLCT bands to examine the benefit of the cooperatively binding phosphonate and carboxylate groups (Figure 4). It was found that ca. 80% of **1** desorbed from the surface within 1 h, although a lower rate of desorption was measured thereafter. This rapid desorption indicates that the dye was very weakly bound, plausibly because of poor carboxylate binding on account of the mesityl *p*-methyl groups. Complex **2**, for which the carboxylate anchoring group could bind more strongly than that of **1**, showed ca. 55% surface desorption within 2 h. The rate of desorption for **3** was lower than that of **2**, yet still only half the original surface coverage was measured after 4 h. We had anticipated that a higher fraction of **3** would be maintained on the surface, although similar desorption rates at neutral pH have been documented for related systems bearing two phosphonate groups.^{16,17,20} It

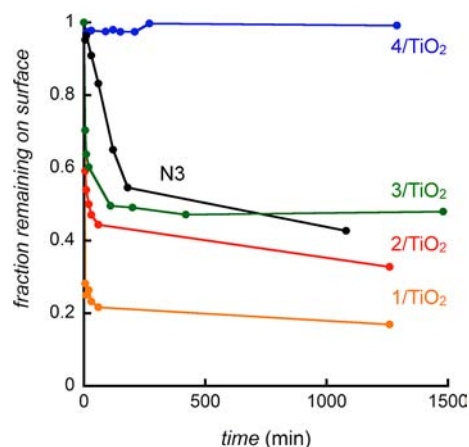


Figure 4. Temporal stabilities of 1–4/TiO₂ submerged in water at pH 7.0. Data for N3 are also shown to highlight the enhanced stability engendered by the cooperatively binding anchoring groups of 4.

was therefore rewarding to find that 4/TiO₂ revealed no evidence of dye desorption over the same period of time. Indeed, the fraction of 4 on the surface was found to remain essentially static over 20 days under said conditions. This result indicates that the cooperative action of the three anchoring groups has a positive effect in stabilizing the dye on the surface. In contrast, substrates stained with N3 led to a loss of ca. 50% surface coverage within 2 h.

This study has demonstrated a simple molecular design strategy for exploiting the favorable properties of distinctive anchoring groups. The placement of carboxylates on the ligand responsible for electron communication with the surface and strongly binding phosphonates between the surface and the opposing ligand achieves both charge transfer and a robust dye/TiO₂ motif. This widely applicable strategy has far-reaching implications for the sensitization of semiconducting materials, particularly in aqueous media. Future studies will be focused on demonstrating this strategy in the context of (photo)-electrocatalytic schemes and developing more strongly absorbing dyes in order to achieve higher PCEs in the DSSC.

■ ASSOCIATED CONTENT

📄 Supporting Information

Full experimental, synthetic, and structural details. This material is available free of charge via the Internet at <http://pubs.acs.org>.

■ AUTHOR INFORMATION

Corresponding Author

cberling@ucalgary.ca

Notes

The authors declare no competing financial interest.

■ ACKNOWLEDGMENTS

C.P.B. is grateful for support from the Natural Science and Engineering Research Council, Canada Research Chairs, Canadian Foundation for Innovation, Canada School of Energy and Environment, and the Alfred P. Sloan Foundation.

■ REFERENCES

- (1) Hagfeldt, A.; Boschloo, G.; Sun, L.; Kloo, L.; Pettersson, H. *Chem. Rev.* **2010**, *110*, 6595.
- (2) Green, M. A.; Emery, K.; Hishikawa, Y.; Warta, W. *Prog. Photovoltaics* **2010**, *18*, 144.

(3) Nguyen, P. T.; Andersen, A. R.; Skou, E. M.; Lund, T. *Sol. Energy Mater. Sol. Cells* **2010**, *94*, 1582.

(4) Asghar, M. I.; Miettunen, K.; Halme, J.; Vahermaa, P.; Toivola, M.; Aitola, K.; Lund, P. *Energy Environ. Sci.* **2010**, *3*, 418.

(5) Wang, M.; Moon, S.-J.; Xu, M.; Chittibabu, K.; Wang, P.; Cevey-Ha, N.-L.; Humphry-Baker, R.; Zakeeruddin, S. M.; Grätzel, M. *Small* **2010**, *6*, 319.

(6) Yanagida, S.; Yu, Y.; Manseki, K. *Acc. Chem. Res.* **2009**, *42*, 1827.

(7) Nguyen, P. T.; Degn, R.; Nguyen, H. T.; Lund, T. *Sol. Energy Mater. Sol. Cells* **2009**, *93*, 1939.

(8) Bomben, P. G.; Robson, K. C. D.; Sedach, P. A.; Berlinguette, C. P. *Inorg. Chem.* **2009**, *48*, 9631.

(9) Bomben, P. G.; Robson, K. C. D.; Koivisto, B. D.; Berlinguette, C. P. *Coord. Chem. Rev.* **2012**, *256*, 1438.

(10) Bomben, P. G.; Gordon, T. J.; Schott, E.; Berlinguette, C. P. *Angew. Chem., Int. Ed.* **2011**, *50*, 10682.

(11) Gao, F.; Wang, Y.; Shi, D.; Zhang, J.; Wang, M.; Jing, X.; Humphry-Baker, R.; Wang, P.; Zakeeruddin, S. M.; Grätzel, M. *J. Am. Chem. Soc.* **2008**, *130*, 10720.

(12) Galoppini, E. *Coord. Chem. Rev.* **2004**, *248*, 1283.

(13) Hanson, K.; Brennaman, M. K.; Luo, H. L.; Glasson, C. R. K.; Concepcion, J. J.; Song, W. J.; Meyer, T. J. *ACS Appl. Mater. Interfaces* **2012**, *4*, 1462.

(14) Bae, E. Y.; Choi, W. Y.; Park, J. W.; Shin, H. S.; Kim, S. B.; Lee, J. S. *J. Phys. Chem. B* **2004**, *108*, 14093.

(15) Gillaizeau-Gauthier, I.; Odobel, F.; Alebbi, M.; Argazzi, R.; Costa, E.; Bignozzi, C. A.; Qu, P.; Meyer, G. J. *Inorg. Chem.* **2001**, *40*, 6073.

(16) Bae, E.; Choi, W. *J. Phys. Chem. B* **2006**, *110*, 14792.

(17) Park, H.; Bae, E.; Lee, J. J.; Park, J.; Choi, W. *J. Phys. Chem. B* **2006**, *110*, 8740.

(18) Ernstorfer, R.; Gundlach, L.; Felber, S.; Storck, W.; Eichberger, R.; Willig, F. *J. Phys. Chem. B* **2006**, *110*, 25383.

(19) Mulhern, K. R.; Orchard, A.; Watson, D. F.; Detty, M. R. *Langmuir* **2012**, *28*, 7071.

(20) Hanson, K.; Brennaman, M. K.; Ito, A.; Luo, H.; Song, W.; Parker, K. A.; Ghosh, R.; Norris, M. R.; Glasson, C. R. K.; Concepcion, J. J.; Lopez, R.; Meyer, T. J. *J. Phys. Chem. C* **2012**, *116*, 14837.

(21) Brown, D. G.; Sanguantrakun, N.; Schulze, B.; Schubert, U. S.; Berlinguette, C. P. *J. Am. Chem. Soc.* **2012**, *134*, 12354.

(22) DFT calculations were performed using the B3LYP hybrid functional with the pseudopotential LANL2DZ basis set for Ru and the 6-31G* basis set for all other atoms.

(23) Robson, K. C. D.; Bomben, P. G.; Berlinguette, C. P. *Dalton Trans.* **2012**, *41*, 7814.

(24) Finnie, K. S.; Bartlett, J. R.; Woolfrey, J. L. *Langmuir* **1998**, *14*, 2744.

(25) Zhang, Z. P.; Zakeeruddin, S. M.; O'Regan, B. C.; Humphry-Baker, R.; Grätzel, M. *J. Phys. Chem. B* **2005**, *109*, 21818.

(26) Suto, K.; Konno, A.; Kawata, Y.; Tasaka, S.; Sugita, A. *Chem. Phys. Lett.* **2012**, *536*, 45.

(27) Bazzan, G.; Deneault, J. R.; Kang, T.-S.; Taylor, B. E.; Durstock, M. F. *Adv. Funct. Mater.* **2011**, *21*, 3268.

(28) Ganbold, E.-O.; Lee, Y.; Lee, K.; Kwon, O.; Joo, S.-W. *Chem.—Asian J.* **2010**, *5*, 852.